PCCP

PAPER

View Article Online
View Journal | View Issue

Cite this: *Phys. Chem. Chem. Phys.*, 2025, **27**, 1473

Ab initio Auger spectrum of the ultrafast dissociating $2p_{3/2}^{-1}\sigma^*$ resonance in HCl†

Mateja Hrast, *[ab] Marko Ljubotina [b] and Matjaž Žitnik*[ac]

Received 27th September 2024,
Accepted 10th December 2024

DOI: 10.1039/d4cp03727h

rsc.li/pccp

We present an *ab initio* theoretical method to calculate the resonant Auger spectrum in the presence of ultrafast dissociation. The method is demonstrated by deriving the L-VV resonant Auger spectrum mediated by the $2p_{3/2}^{-1}\sigma^*$ resonance in HCl, where the electronic Auger decay and nuclear dissociation occur on the same time scale. The Auger decay rates are calculated within the one-center approximation and are shown to vary significantly with the inter-nuclear distance. A quantum-mechanical description of dissociation is effectuated by propagating the corresponding Franck–Condon factors. The calculated profiles of Auger spectral lines resemble those of atomic Auger decay but here the characteristic tails extend towards lower electron kinetic energies, which reflect specific features of the potential energy curves. The presented method can describe the resonant Auger spectrum for an arbitrary speed of dissociation and simplifies to known approximations in the limiting cases.

1 Introduction

The concept of ultrafast dissociation (UFD) was first proposed in 1986 by Morin and Nenner in the analysis of their experimental results on the HBr molecule.[1] They concluded that the Auger decay of the 3d hole in a molecule, resonantly excited to an anti-bonding state, mostly occurs after the neutral dissociation of HBr has taken place, as the observed electron spectrum was similar to that emitted by the 3d hole in atomic Br. Atomic lines, demonstrating dissociation on a time scale shorter than Auger decay, were later found in the spectra of other molecules, as well, typically upon excitation of an electron from an inner to an antibonding molecular orbital.[2–7]

Despite the abundance of experimental data,[8–17] the competition between UFD and Auger decay still lacks theoretical description, which would thoroughly follow the UFD driven changes of electronic decay from the molecular to purely atomic environment. Due to numerous degrees of freedom, the molecular Auger spectra are rather complex with different overlapping features, which makes theoretical modelling of even the simplest molecules challenging. While calculations of the electronic structure of the molecular ground state and valence-excited states are now performed routinely, accurate methods to describe the asymptotically free Auger electron wave in a true molecular potential have only emerged recently.[18–21]

In a recent work, Kokkonen *et al.*[4] studied UFD in chloromethanes with a 2p vacancy on chlorine. Clear experimental evidence of UFD was found in the lightest species CH_3Cl, while no clear UFD signal was observed in the heaviest CCl_4, although the initial dynamics within the Franck–Condon region is similar for both.[22] A simple Mulliken analysis showed that the charge redistribution triggered by dissociation is faster in heavier chloromethanes and may affect the electronic wavefunctions significantly during the dissociation. However, this analysis alone is insufficient to directly explain the difference between the observed $2p_{3/2}^{-1}\sigma^*$ resonant Auger (RA) spectra of different chloromethanes. Clearly, Auger rate calculations that account for the variation of the electronic molecular states during dissociation are required to explain the observation.

An example of the competition between UFD and Auger decay in the HCl molecule is illustrated in Fig. 1. After exciting an electron from the 2p core orbital of the chlorine atom to the antibonding LUMO σ^* (red dashed arrow), the molecule finds itself in an ultrafast dissociating state, represented by the top potential energy curve (PEC). As the system travels along the PEC, Auger decay can occur at any point during the dissociation (orange arrows) or later in the separated atoms (purple arrow), placing the molecule (or in the separated case, the chlorine atom) in the ionized state with two vacancies in the valence shell. Unlike in fluorescence decay, PECs of the initial and final states of the Auger decay are never parallel, so the energy difference between the PECs varies with inter-nuclear distance, and the corresponding Auger spectral line is non-trivially broadened.

[a] *Jožef Stefan Institute, Jamova cesta 39, 1000 Ljubljana, Slovenia. E-mail: matjaz.zitnik@ijs.si*
[b] *Institute of Science and Technology Austria (ISTA), Am Campus 1, 3400 Klosterneuburg, Austria. E-mail: mateja.hrast@ist.ac.at*
[c] *Faculty of Mathematics and Physics, University of Ljubljana, Jadranska 31, 1000 Ljubljana, Slovenia*

† Electronic supplementary information (ESI) available: Derivation of the Auger decay rates. See DOI: https://doi.org/10.1039/d4cp03727h

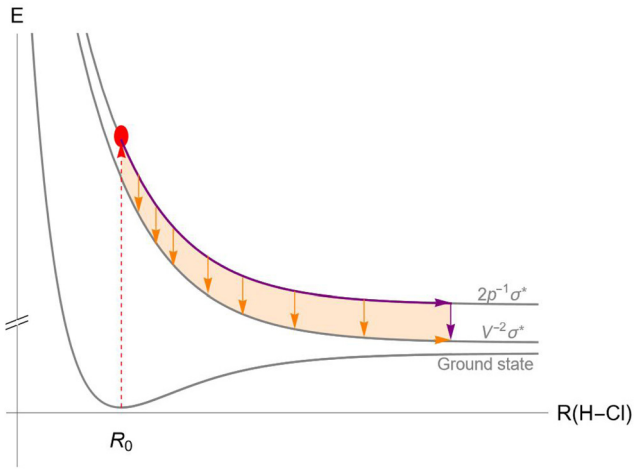

Fig. 1 Scheme of the potential energy curves of the ground (bottom curve), initial $2p^{-1}\sigma^*$ (top curve) and final $v^{-2}\sigma^*$ (middle curve) states of the Auger decay in the HCl molecule. Photoexcitation (red arrow) triggers dissociation along the PEC of the initial state (purple). Auger decay happens anytime during the dissociation (orange arrows), with both the decay rate and the Auger electron energy depending on the inter-nuclear distance R. The vertical purple arrow represents the Auger decay in the atomic limit.

This exact process had already been extensively studied experimentally[2,6,23–27] but the only attempt that we are aware of to model the mixed molecular-atomic nature of Auger line-shapes is that of Kukk *et al.*[28] (later reproduced by Menzel *et al.*[3]). They used a simple exponential interpolation through potential energy points from ref. 29. The Auger line shapes were generated using a Monte-Carlo procedure, assuming a vibrational ground state and relying on a semi-classical description of dissociation along the PEC of the $2p^{-1}\sigma^*$ state, based on the experimentally known parameters. While they have assigned the Auger kinetic energy at the moment of emission to the difference in the corresponding PECs, they have assumed the Auger decay rate to be independent of the inter-nuclear distance. Their work was later used by Kivimäki *et al.* to fit the angular-dependent experimental spectra.[24] They used a combination of a pseudo-Voigt profile for the atomic peak and a symmetric Gaussian for the molecular tail, which adequately described the measured spectra.

There are other existing approaches to treat the UFD and Auger decay simultaneously, however, they rely on different simplifications, which are not valid for the decay of the Cl 2p hole. For example, Goldsztejn *et al.*[30] treated the 1s photoionization and excitation in HCl. They derived quantum-mechanical expressions for the Auger cross-section within the Franck–Condon region. However, their approach is only applicable for small deviations from the ground state geometry, which is sufficient to describe the K-LL Auger decay, which occurs on about 8 times shorter time scale than the decay of the Cl 2p hole.[31] Another approach was suggested and applied to the HF molecule by Pahl *et al.*,[32] where only the nuclear wavefunction was propagated in time, while the electronic part was assumed to be independent of the nuclear coordinates. However, the recent work of Kokkonen *et al.*[4] shows that the electronic part must play an important role in the case of the L-VV Auger decay of the 2p vacancy in chloromethanes. Inhester *et al.*[33] combined a model of classically-propagating nuclei with an explicit integration of coupled Schrödinger equations to describe the electron continuum wavefunction at different molecular geometries. Their model was recently used to describe the measured Auger spectra of water.[14,17] The most recent theoretical approach by Tenorio *et al.*[34] employed a combination of a restricted-active-space perturbation theory and molecular dynamics simulations to describe the effect of UFD in ozone. Their nuclear dynamics calculation is based on a statistical description of the initial geometry and adiabatic propagation in small time steps. Although the works of Inhester *et al.* and Tenorio *et al.* accurately capture the main features of the measured Auger spectra, we show in this work that a quantum-mechanical description of nuclear dynamics is needed to model specifically asymmetric line-shapes produced by UFD.

Several theoretical studies have also been performed to describe the non-resonant Auger decay following 2p photoionization of HCl. The most recent is that by Kivilompolo *et al.*,[9] who performed a non-relativistic *ab initio* calculation of the Auger electron spectra in several chlorine-containing molecules. They used a Hartree–Fock based method, the one-center approximation (which has been successfully applied to the HCl molecule before[35,36]) and also included configuration interaction and lifetime vibrational interference. However, their treatment of dissociation of the $2p^{-1}$ molecular ion was derived solely from the shape of the PEC near the equilibrium distance, because the dissociation is slower than in the $2p^{-1}\sigma^*$ case.

This paper presents a relatively simple and robust, *ab initio* approach for calculating the Auger spectrum of an ultrafast dissociating molecular state that follows the evolution of the molecular state all along the potential energy curve. First, a quantum-chemical calculation of PECs for all molecular states is required. Next, the one-center method[37] is employed to project the evolving molecular orbitals onto the atom with a localized core hole, which gives the largest contribution to the Auger decay rate. These projections are then expanded in the atomic orbitals of the atom with the core–hole. Assuming frozen spectator orbitals at different stages of dissociation, the expressions for the Auger decay rates reduce to a sum of atomic-like terms, which are relatively simply evaluated. The quantum-mechanical approach of Gelmukhanov and Ågren[38] is adapted to our case to treat nuclear dynamics. Partial amplitudes are derived in terms of Franck–Condon factors using a quasiclassical propagator. To obtain the spectral lines, the contributions are integrated over the energy range of each final state, which generates the characteristic shape for a given Auger transition. Finally, the spectral lines of all final states are summed into the total Auger spectrum. To illustrate the method we present the calculation of the resonant Auger electron spectrum of the $2p \rightarrow \sigma^*$ excitation in the HCl molecule.

This paper is organized as follows. In Section 2, we present the method of calculation, including the calculation of the

Table 1 The molecular states of the HCl^+ ion with two holes in the valence orbitals (4σ, 5σ and 2π) and a σ* electron. The expression $^{2S_{vv'}+1}\Lambda$ gives the coupling of the unpaired vv′ electrons. Column 4 gives the expression of state energies in terms of the single-configuration state energies for states not taken from Pradhan *et al.*[29] Column 5 gives the state dissociation limits. States (6)–(11) and state (14) are doubly degenerate due to the degeneracy of the π_x/π_y orbitals

Configuration	f	$^{2S+1}\Lambda^{+/-}\left(^{2S_{vv'}+1}\Lambda\right)$	State energy	Dissociation limit
$4\sigma^{-2}\sigma^*$	(1)	$^2\Sigma^+(^1\Sigma^+)$	$E_{4\sigma^{-2}\sigma^*(\uparrow)}$	$Cl^+([3s^{-2}]^1S) + H(^2S)$
$5\sigma^{-2}\sigma^*$	(2)	$^2\Sigma^+(^1\Sigma^+)$	Pradhan $(3)^2\Sigma^+$	$Cl^+([3p^{-2}]^1S) + H(^2S)$
$4\sigma^{-1}5\sigma^{-1}\sigma^*$	(3)	$^2\Sigma^+(^1\Sigma^+)$	$\frac{1}{2}\left(E_{4\sigma(\uparrow)5\sigma(\downarrow)\sigma^*(\uparrow)} + E_{4\sigma(\downarrow)5\sigma(\uparrow)\sigma^*(\uparrow)}\right)$	$Cl^+([3s^{-1}\ 3p^{-1}]^1P) + H(^2S)$
	(4)	$^2\Sigma^+(^3\Sigma^+)$	$\frac{2}{3}E_{4\sigma(\downarrow)5\sigma(\downarrow)\sigma^*(\uparrow)} + \frac{1}{6}\left(E_{4\sigma(\uparrow)5\sigma(\downarrow)\sigma^*(\uparrow)} + E_{4\sigma(\downarrow)5\sigma(\uparrow)\sigma^*(\uparrow)}\right)$	$Cl^+([3s^{-1}\ 3p^{-1}]^3P) + H(^2S)$
	(5)	$^4\Sigma^+(^3\Sigma^+)$	$E_{4\sigma(\uparrow)5\sigma(\uparrow)\sigma^*(\uparrow)}$	$Cl^+([3s^{-1}\ 3p^{-1}]^3P) + H(^2S)$
$4\sigma^{-1}2\pi^{-1}\sigma^*$	(6)	$^2\Pi(^1\Pi)$	$\frac{1}{2}\left(E_{4\sigma(\uparrow)2\pi_x(\downarrow)\sigma^*(\uparrow)} + E_{4\sigma(\downarrow)2\pi_x(\uparrow)\sigma^*(\uparrow)}\right)$	$Cl^+([3s^{-1}\ 3p^{-1}]^1P) + H(^2S)$
	(7)	$^2\Pi(^3\Pi)$	$\frac{2}{3}E_{4\sigma(\downarrow)2\pi_x(\downarrow)\sigma^*(\uparrow)} + \frac{1}{6}\left(E_{4\sigma(\uparrow)2\pi_x(\downarrow)\sigma^*(\uparrow)} + E_{4\sigma(\downarrow)2\pi_x(\uparrow)\sigma^*(\uparrow)}\right)$	$Cl^+([3s^{-1}\ 3p^{-1}]^3P) + H(^2S)$
	(8)	$^4\Pi(^3\Pi)$	$E_{4\sigma(\uparrow)2\pi_x(\uparrow)\sigma^*(\uparrow)}$	$Cl^+([3s^{-1}\ 3p^{-1}]^3P) + H(^2S)$
$5\sigma^{-1}2\pi^{-1}\sigma^*$	(9)	$^2\Pi(^1\Pi)$	Pradhan $(3)^2\Pi$	$Cl^+([3p^{-2}]^1D) + H(^2S)$
	(10)	$^2\Pi(^3\Pi)$	Pradhan $(2)^2\Pi$	$Cl([3p^{-1}]^2P) + H^+$
	(11)	$^4\Pi(^3\Pi)$	Pradhan $^4\Pi$	$Cl^+([3p^{-2}]^3P) + H(^2S)$
$2\pi^{-2}\sigma^*$	(12)	$^2\Sigma^+(^1\Sigma^+)$	Pradhan $(2)^2\Sigma^+$	$Cl^+([3p^{-2}]^1D) + H(^2S)$
	(13)	$^2\Sigma^-(^3\Sigma^-)$	Pradhan $^2\Sigma^-$	$Cl^+([3p^{-2}]^3P) + H(^2S)$
	(14)	$^2\Delta(^1\Delta)$	Pradhan $^2\Delta$	$Cl^+([3p^{-2}]^1D) + H(^2S)$
	(15)	$^4\Sigma^-(^3\Sigma^-)$	Pradhan $^4\Sigma^-$	$Cl^+([3p^{-2}]^3P) + H(^2S)$

PECs in Section 2.1, the calculation of the Auger decay rates in Section 2.2, while Section 2.3 presents the treatment of nuclear dynamics of the molecule, which undergoes Auger decay at the same time. This gives the total Auger electron spectrum, which is presented and discussed in Section 3, including a comparison with the experimental spectrum. Finally, Section 4 gives the conclusions and suggests possible improvements in the presented method.

2 Method

2.1 Potential energy curves

To account for the Auger decay which can occur throughout the dissociation process the PECs up to large inter-nuclear distances are required for all the states involved in the RA decay. A method to calculate accurate PECs up to large inter-nuclear distances with extensive configuration mixing was presented by Pradhan *et al.*,[29] who reported PECs for the lowest 12 states of the HCl^+ ion. To obtain reasonably good PECs for the remaining states we have limited the description of molecular states to linear combinations of single-configuration electronic states with different spin projections. StoBe deMon implementation of the density functional theory (DFT) method based on the Kohn–Sham equations[39] was used to calculate molecular orbitals. The PD86 PBE non-local exchange–correlation functional of Perdew and Wang[40,41] was used. A flexible augmented correlation consistent polarised valence quadruple zeta basis set AugccPVQZ[42] with two additional diffuse s, p, and d functions was used on the chlorine atom, while the ii_iglo[43] basis set was used on the hydrogen atom. The energy convergence threshold for the self-consistent field procedure was 10^{-7} a.u., the grid consisted of 70 and 50 radial points on chlorine and hydrogen atoms, respectively, and 26 angular points per radial shell.

The initial state $2p^{-1}\sigma^*$ of the Auger decay is known to submit to a strong spin–orbit coupling, as well as to the molecular field splitting.[36] To account for both effects, we calculated the PECs of the $2p_{x,y,z}{}^{-1}\sigma^*$ states and applied the method proposed by Gel'mukhanov[44] at each point of the PEC. The method treats spin–orbit coupling of the 2p core hole only and the Hamiltonian in the molecular basis is directly diagonalized to simultaneously account for the molecular field splitting. Our results at the equilibrium geometry agree with those of Aksela *et al.*[23] and the expected splitting of the $2p_{3/2}$ and $2p_{1/2}$ atomic lines is verified in the dissociation limit. This work focuses on the calculation of the Auger spectrum emitted from the lowest $2p_{3/2}{}^{-1}\sigma^*$ electronic state of HCl in the presence of a fast neutral dissociation.

The final states of the Auger process $v^{-1}v'^{-1}\sigma^*$, with the two valence shell vacancies v and v′ in either 4σ, 5σ or 2π molecular orbitals, and a spectator electron in the σ* orbital, are given in Table 1. For some of the states, PECs are reported in ref. 29, while others were calculated from linear combinations of single-configuration states, which satisfy the spin, angular momentum and symmetry requirements of true molecular states. Even though these wavefunctions can be very complicated, the final state energies are straightforwardly expressed in terms of energies for electronic configurations with different distributions of spin projections (see column 4 of Table 1).

Although DFT produces PECs of reasonably accurate shapes, we find that in our implementation the energy differ-

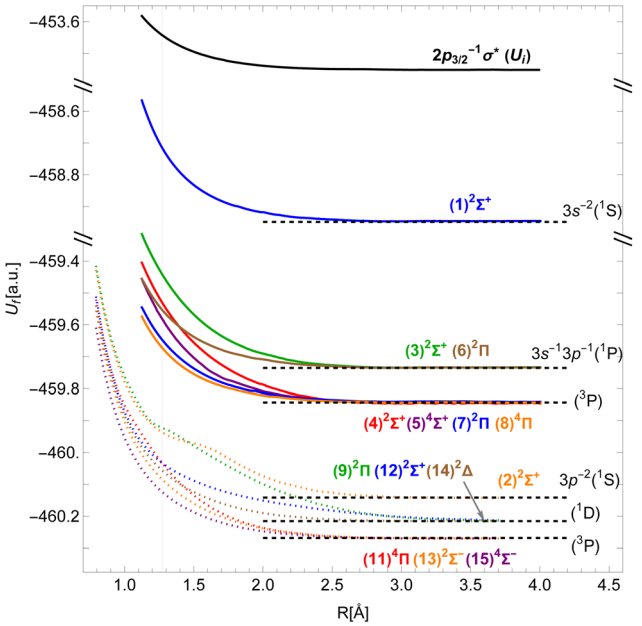

Fig. 2 Potential energy curves of the $2p_{3/2}{}^{-1}\sigma^*$ state in HCl (black) and of the $v^{-1}v'^{-1}\sigma^*$ states of the HCl^+ molecular ion (colors; dotted curves taken from Pradhan *et al.*[29]). Horizontal dashed lines denote the energies of the Cl^+ ionic states. The vertical line shows the equilibrium inter-nuclear distance of HCl.

ences between the asymptotic states are not entirely reliable. To improve this, we assign each molecular state its dissociation limit using the Wigner–Witmer rules.[45] As indicated in the last column of Table 1, the limits correspond to excited states of the Cl^+ ion with two 3s and/or 3p vacancies. Our PECs are shifted vertically to match the energy differences of the corresponding atomic states, taken from ref. 46, in the dissociation limit. The resulting PECs are shown in Fig. 2.

The shape of the initial state's PEC governs the dynamics of dissociation, as discussed in Section 2.3. The differences between the initial and final states' PECs at different inter-nuclear distances correspond to the kinetic energies of the Auger electron.

2.2 Auger transition rates

The Auger transition rate from an initial state Ψ_i with the energy E_i to a final state Ψ_f of the molecular ion plus a continuum electron ψ_ε with the respective energies E_f and ε in atomic units is

$$A_{i\to f} = 2\pi\left|\left\langle \Psi_f\psi_\varepsilon\left|\sum_{i>j}\frac{1}{r_{ij}}\right|\Psi_i\right\rangle\right|^2\delta(E_i - E_f - \varepsilon). \qquad (1)$$

The initial state Ψ_i is the $2p^{-1}\sigma^*$ electronic state of HCl with total spin S' and projection $M_{S'}$, antisymmetrized with respect to the exchange of any two electrons.

The final state Ψ_f consists of a pair of vacancies vv' in the valence shell and an electron in the σ^* orbital, coupled to total spin S, its projection M_S, and projection Λ of the orbital angular momentum on the molecular axis. The unpaired vv' electrons are coupled to a spin $S_{vv'}$ with a projection $M_{S_{vv'}}$, and the same orbital angular momentum projection Λ. Within the one-center approximation (see below) the free Auger electron with spin projection $m_{s\varepsilon}$ is approximated by the sum of partial waves

$$\psi_\varepsilon = |m_{s\varepsilon}\rangle\sum_{\ell_\varepsilon m_\varepsilon}|\ell_\varepsilon m_\varepsilon\rangle \qquad (2)$$

centered on the Cl atom. Continuum channels up to $\ell_\varepsilon = 3$ were included in our calculations.

The sum in eqn (1) runs over all electron pairs and $r_{ij} = |\vec{r}_i - \vec{r}_j|$ denotes the inter-electronic distance. We are interested in the Auger rate (1) averaged over the initial spin S', spin projection $M_{S'}$ and the projection m of the orbital angular momentum of the core–hole, as well as summed over the final spin projections M_S and $m_{s\varepsilon}$. Furthermore, we take into account that Auger transitions conserve total spin and its projection, as well as the projection of the total orbital angular momentum. Then the averaged Auger decay rate integrated over the electron emission angle can be written as:

$$\begin{aligned}\tilde{A}_f &= \frac{\pi}{12}(\mathscr{S}(0,S_{vv'},S) + 3\mathscr{S}(1,S_{vv'},S))\\ &\times\sum_{m,\ell_\varepsilon,m_\varepsilon}\left|\left\langle 2p\ell_\varepsilon m_\varepsilon\left|\frac{1}{r_{12}}\right|vv';\Lambda,S_{vv'}\right\rangle\right.\\ &\left.+(-1)^{S_{vv'}}\left\langle 2p\ell_\varepsilon m_\varepsilon\left|\frac{1}{r_{12}}\right|v'v;\Lambda,S_{vv'}\right\rangle\right|^2.\end{aligned} \qquad (3)$$

To obtain this result we took a single set of orthonormal molecular orbitals to represent the antisymmetrized initial and final states. In the case of HCl, only the σ^* molecular orbital changes notably between the initial and final states, but as the overlap of the two remains reasonably large along the dissociation path, an approximation with frozen spectator orbitals is still acceptable.

The two matrix elements in eqn (3) are the direct and exchange two-electron integrals of the given pairs of spin–orbitals (often denoted $J_{vv'}$ and $K_{vv'}$), and the spin factor $\mathscr{S}$ is given by

$$\begin{aligned}\mathscr{S}(S',S_{vv'},S) = &\frac{2}{2S'+1}\sum_{M_{S'},M_S,m_{s\varepsilon}}\left[\sum_{m_s,M_{S_{vv'}},m_\sigma}\left\langle\frac{1}{2}m_s\frac{1}{2}m_\sigma\middle|S'M_{S'}\right\rangle\right.\\ &\left.\times\left\langle S_{vv'}M_{S_{vv'}}\frac{1}{2}m_\sigma\middle|SM_S\right\rangle\left\langle\frac{1}{2}m_s\frac{1}{2}m_{s\varepsilon}\middle|S_{vv'}M_{S_{vv'}}\right\rangle\right]^2.\end{aligned} \qquad (4)$$

For the derivation of eqn (3) and (4) see the ESI.†

To calculate the two-electron integrals from eqn (3) we employ the one-center method,[37] which only retains the terms in the molecular orbital expansion that are centered on the same atom as the core–hole. This has proven successful for a well-localized core–hole, since the largest contributions to the decay rate integral come from the vicinity of the core–hole. Furthermore, in the vicinity of the core–hole the molecular orbitals can be well described by a linear combination of atomic orbitals centered on the atom containing the hole.

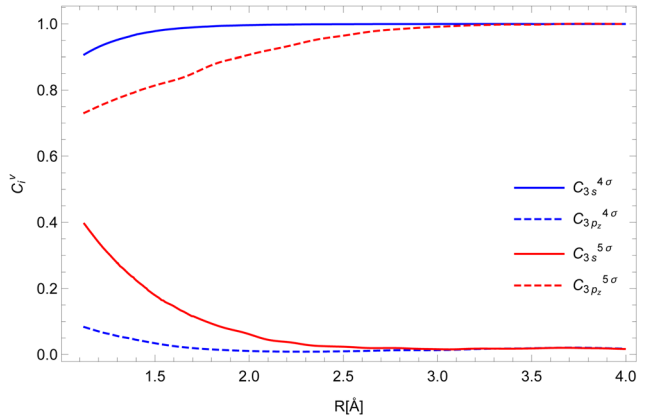

Fig. 3 The expansion coefficients C_i^v of the valence shell v into atomic orbitals i for the 4σ (blue) and 5σ (red) orbitals.

If the expansion coefficients C_i^v (i runs over the atomic orbitals) of the valence orbitals v are known, the work of Chelkowska and Larkins[35] gives the necessary data to calculate the sums in eqn (3). As the molecular orbitals evolve during the dissociation, the corresponding coefficients C_i^v, also evolve, which we have determined as a function of inter-nuclear distance using the least squares method. The atomic orbitals of Cl were calculated by the Hartree–Fock method using the ATSP atomic structure calculation package.[47] The two 2π molecular orbitals were found to directly correspond to the $2p_x$ and $2p_y$ orbitals of Cl throughout dissociation. The 4σ and 5σ molecular orbitals have contributions of both 3s and $3p_z$ atomic orbitals at the equilibrium distance and change into pure 3s and $3p_z$ respectively in the atomic limit. Consequently, their $C^v_{3s/3p_z}$ coefficients depend on the inter-nuclear distance, as shown in Fig. 3.

This expansion allowed for a straightforward application of the $I^{2p,\varepsilon}_{vv'}\left({}^{2S_{vv'}+1}\Lambda\right)$ non-resonant rates from Chelkowska and Larkins[35] (see eqn (7) therein) in the calculation of the resonant Auger rates. Using atomic orbitals and continuum waves calculated *ab initio* with the atomic code GRASP2K,[48] we have reevaluated the Slater integrals R^k between the four radial parts of the atomic orbitals participating in the Auger decay. We found good agreement with the values from Table II of Chelkowska and Larkins.[35]

Our results for the Auger decay rates to the $v^{-1}v'^{-1}\sigma^*$ final states as a function of inter-nuclear distance are presented in Fig. 4. As the expansion into atomic orbitals in principle depends on inter-nuclear distance, so does the Auger rate, though each final state is affected differently. Those without 4σ or 5σ vacancies exhibit constant rates in our model (dashed lines). The strongest effect can be seen for the states with two 5σ vacancies and $5\sigma^{-1}2\pi^{-1}$ configurations. States with a 4σ vacancy experience a smaller change of the rate because this vacancy is more localized. For all final states the calculation shows an enhancement in the probability for the Auger transition at a larger inter-nuclear distance. The relative change of the rate from the equilibrium position to the separated atoms

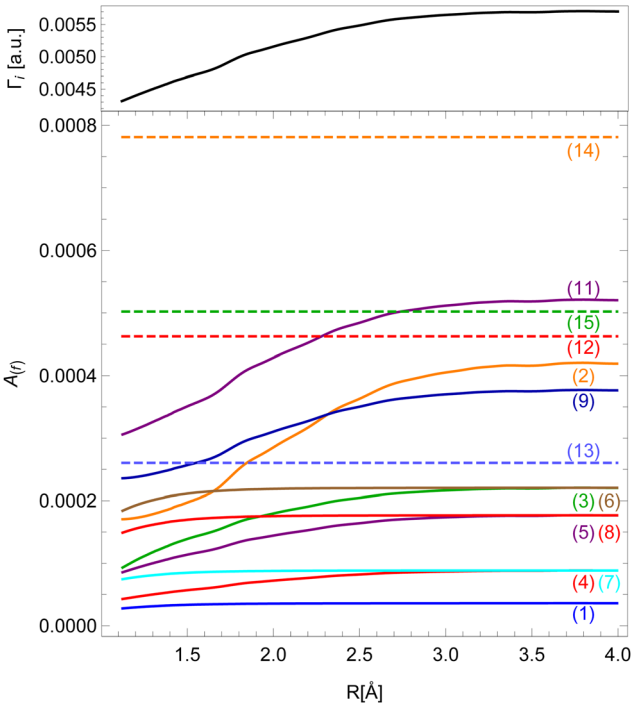

Fig. 4 Dependence of Auger decay rates on the inter-nuclear distance for different final states (colors, see Table 1) and the total decay rate Γ_i (black).

limit can be up to 100% which makes previous assumptions about a constant Auger rate questionable.[28]

Even though the transition rates calculated by the method described above are averaged over the orbital angular momentum of the core–hole m, we may approximately assign the resulting spectrum to the resonant Auger spectrum of the $2p_{3/2}{}^{-1}\sigma^*$ initial state. The sum of the transition rates into all final states gives the total decay rate Γ_i of the initial state, which is shown on top of Fig. 4.

Finally, we note that while all other final states dissociate into a chlorine ion and a neutral hydrogen in the ground state, the $(10)^2\Pi$ final state dissociates into neutral chlorine and the hydrogen ion, which means the decay must occur *via* the inter-Coulombic decay (ICD) channel and cannot be described by the one-center method. Therefore this work does not consider the contribution of the $(10)^2\Pi$ state to the Auger spectrum.

2.3 Nuclear dynamics

Within the Born–Oppenheimer approximation, the molecular wavefunction is split into the electronic (ψ) and nuclear part (χ). Treating the resonant Auger decay as a two-step process, photoexcitation by a photon with energy ω and Auger decay by ejecting an electron with energy ε, the scattering amplitude into final state f is given by[38]

$$F_f(\omega,\varepsilon) = \int \mathrm{d}E_i \frac{\langle\psi_f\psi_\varepsilon|V|\psi_i\rangle\langle\chi_f^q \mid \chi_i^k\rangle\langle\psi_i|D|\psi_0\rangle\langle\chi_i^k \mid \chi_0\rangle}{\omega - E_i + i\Gamma_i/2}, \quad (5)$$

where the integral runs over the range of initial state energies.

The dipole matrix element $D_{i0} = \langle\psi_i|D|\psi_0\rangle$ in (5) has a constant value for all final states and can be set to 1, when calculating only the spectral shape. The absolute squares of the Coulomb matrix elements $|V_{fi}|^2 = |\langle\psi_f\psi_\varepsilon|V|\psi_i\rangle|^2$ are approximated by $\tilde{A}_f/2\pi$. As the averaged Auger rates are real and non-zero at all inter-nuclear distances we can, up to a sign globally, estimate

$$V_{fi}(R) = \sqrt{\frac{\tilde{A}_f(R)}{2\pi}}. \tag{6}$$

The matrix elements $\langle\chi_f^q|\chi_i^k\rangle$ and $\langle\chi_i^k|\chi_0\rangle$ in eqn (5) are the so-called continuum–continuum (cc) and bound–continuum (bc) Franck–Condon (FC) factors.[49] They are evaluated using the ground state of the harmonic oscillator to represent the nuclear wavefunction of the ground state χ_0, and for the initial and final states, χ_i^k and χ_f^q, the numerical solutions of the Schrödinger equation with the corresponding PEC are employed. The latter are evaluated at the equilibrium energy $E_i = U_i(R_0)$ for the initial state, while the final state energy depends also on the kinetic energy of the Auger electron, $E_f = E_i - \varepsilon$. The corresponding wave vectors are then given by $k = \sqrt{2m_r(U_i(R_0) - U_i(R_\infty))}$ and $q(\varepsilon) = \sqrt{2m_r(U_f(R_t(\varepsilon)) - U_f(R_\infty))}$, respectively, where R_t is the classical turning point for a molecular state with energy E_f on the final state's potential.

The solutions for χ_i and χ_f for a given energy come in pairs, where χ^A behaves as a sine wave in the $R \to \infty$ limit and χ^B as a cosine (see Fig. 5). As the dissociation is described by an outgoing rather than a standing wave, the two solutions must be combined to obtain the nuclear wavefunction of the initial state

$$\chi_i^k(R) = \sqrt{\frac{2}{\pi k\sqrt{m_r}}}\left(\frac{1}{N^A}\chi_i^A(R) + i\frac{1}{N^B}\chi_i^B(R)\right) \tag{7}$$

with the correct asymptotic behaviour. The coefficients N^A and N^B are the amplitudes of χ^A and χ^B in the atomic limit, to ensure proper normalization to the $\delta(k^2 - k'^2)$ function. The nuclear wavefunction of the final state is obtained in a similar way, only that here the kinetic energy of the Auger electron defines the position R_f of the turning point.

Let us now return to eqn (5). We expand the amplitude to the double integral over R and $R' > R$ to get

$$F_f(\omega,\varepsilon) = \int_0^\infty dR\int_R^\infty dR' V_{fi}(R')\chi_f^{q*}(R')G_\omega(R',R)\chi_0(R). \tag{8}$$

As the RA experiment in principle cannot determine at which inter-nuclear distance R the photon was absorbed and at which R' the electron with kinetic energy ε was ejected, the amplitudes of all absorption–emission paths interfere, which is indicated by the form of eqn (8).

To evaluate the Green's function propagator $G_\omega(R', R)$, Gelmukhanov and Ågren[38] assume a semi-classical approximation of χ_i^k and derive the expression

$$G_\omega(R',R) = G_\omega^{(0)}(R',R)\exp\left(-\frac{\Gamma_i}{2}\int_R^{R'}\frac{1}{v(R'')}dR''\right). \tag{9}$$

The velocity v above depends on inter-nuclear distance R'' and is given by

$$v(R'') = \sqrt{\frac{2(U_i(R_0) - U_i(R''))}{m_r}}. \tag{10}$$

The exponentially decaying factor in eqn (9) correlates the absorption point and the emission point, where Γ_i defines how fast the amplitude diminishes when R' is distancing from R.

Instead of using the semi-classical approximation as in the work of Gelmukhanov and Ågren,[38] we use the numerical eigenfunction χ_i^k (see eqn (7)), to estimate the prefactor $G_\omega^{(0)}(R', R) \approx \chi_i^k(R')\chi_i^{k*}(R)$. In addition, we modify the exponential factor in (9) to account for the R-dependence of the decay rate Γ_i, taking it under the integral over R''. Finally, the expression for the RA amplitude becomes

$$\begin{aligned} F_f(\omega,\varepsilon) = &\int_0^\infty dR\int_R^\infty dR' V_{fi}(R')\chi_f^{q*}(R')\chi_i^k(R')\chi_i^{k*}(R) \\ &\times\exp\left(-\frac{1}{2}\int_R^{R'}\frac{\Gamma_i(R'')}{v(R'')}dR''\right)\chi_0(R). \end{aligned} \tag{11}$$

Expression (11) matches the results of Gelmukhanov and Ågren[38] for all limiting cases they consider. Note that the Γ_i, we refer to in our work, signifies the full-width-at-half-maximum (FWHM) of the natural lifetime broadening of the initial state, which is twice larger than the half-width (HWHM) value used by Gelmukhanov and Ågren.[38]

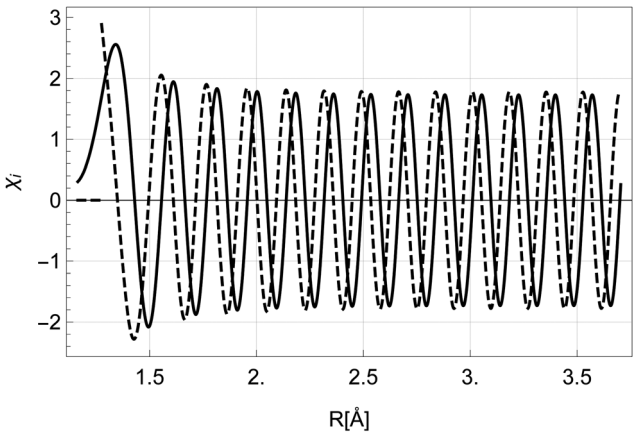

Fig. 5 The nuclear wavefunctions χ_i^A (full) and χ_i^B (dashed) with energy $E_i = U_i(R_0)$ in the initial state. The function χ_i^B diverges at $R < R_0$ and is set to 0 in the classically forbidden region.

3 Results and discussion

The expression for the total resonant Auger cross-section is given by the Fermi golden rule as ref. 50

$$\sigma(\omega,\varepsilon) = 4\pi^2\alpha\omega\sum_f|F_f(\omega,\varepsilon)|^2 \equiv \sum_f\sigma_f(\omega,\varepsilon), \tag{12}$$

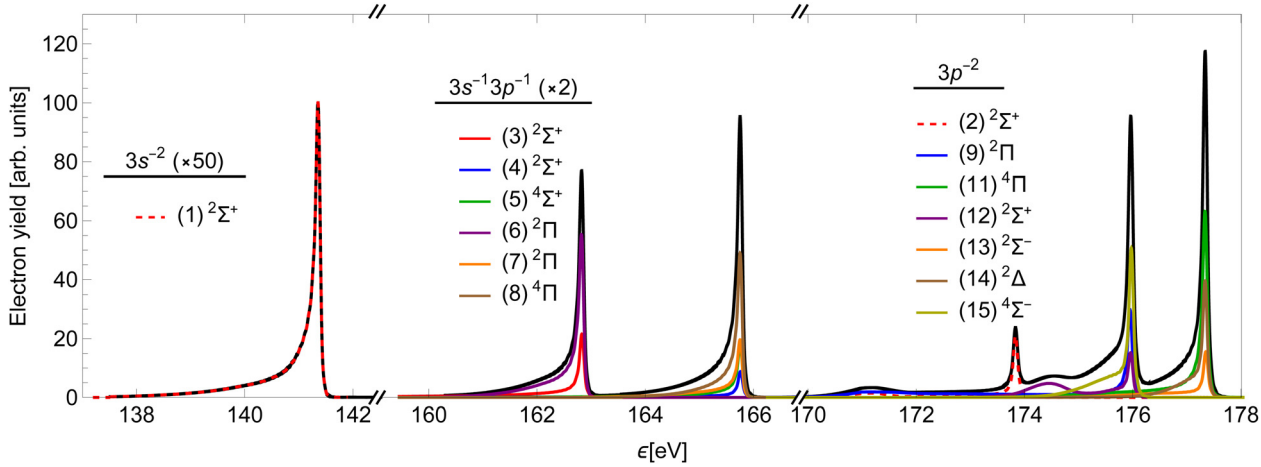

Fig. 6 The calculated resonant L-V^2 Auger electron spectrum of the $2p_{3/2}{}^{-1}\sigma^*$ state of HCl (black) at photon energy $\omega = U_i(R_0)$. The groups are assigned according to the dissociation limits of the final $v^{-1}v'^{-1}\sigma^*$ states, the lower two are vertically scaled for a clearer presentation. Coloured lines show contributions of different final states.

where α is the fine-structure constant and the decay widths Γ_f of the final states are assumed to be much smaller than the width Γ_i of the initial state with a core–hole.

Using the method presented in Section 2, we calculated the partial cross-sections σ_f and summed them into the total Auger spectrum of the $2p_{3/2}{}^{-1}\sigma^*$ state of HCl (see Fig. 6). The spectrum consists of three distinct groups of lines: the one at the lowest ε corresponds to the final states, which dissociate to the $3s^{-2}$ states of Cl^+, the middle to the $3s^{-1}3p^{-1}$ states and the highest to the $3p^{-2}$ states.

The two high-energy parts of the spectrum can be compared to the experimental result of ref. 51, which measured the corresponding Auger spectrum integrated over the emission angle of the Auger electron (Fig. 7). Our calculation fails to capture the relative intensities of the experimental peaks, mostly due to neglecting the effect of spin–orbit (SO) coupling of final states, which would split the right-most ^{3}P peak into three components. The SO interaction splits the peaks without changing the total yield. We verify that the ratio of the total area for the three states converging to ^{3}P with respect to the total area of the peaks converging to ^{1}D in our calculation is reasonably close to that in the experiment. Despite this, we see that our calculation quite accurately reproduces the asymmetric lineshapes in the high-energy part of the spectrum (a) and even some details in the molecular tails. We note specifically the additional peaks at around 175 eV and 178 eV, which are produced by the smaller slope of the PECs (2), (9) and (12) right above the equilibrium R. The lower of the two is slightly wider than in the experiment, which could be caused by small inaccuracies in the PECs. There is an additional feature at around 180 eV, which is not reproduced in our calculation. It probably stems from the predissociation of the vibrational states in the $A^2\sigma^+$ potential, which is caused by the SO interaction with the dissociative $5\sigma^{-1}2\pi^{-14}\Pi$ final state.[29] The low-energy part of the spectrum in panel (b) is over-estimated by our calculation. This indicates a different level of accuracy

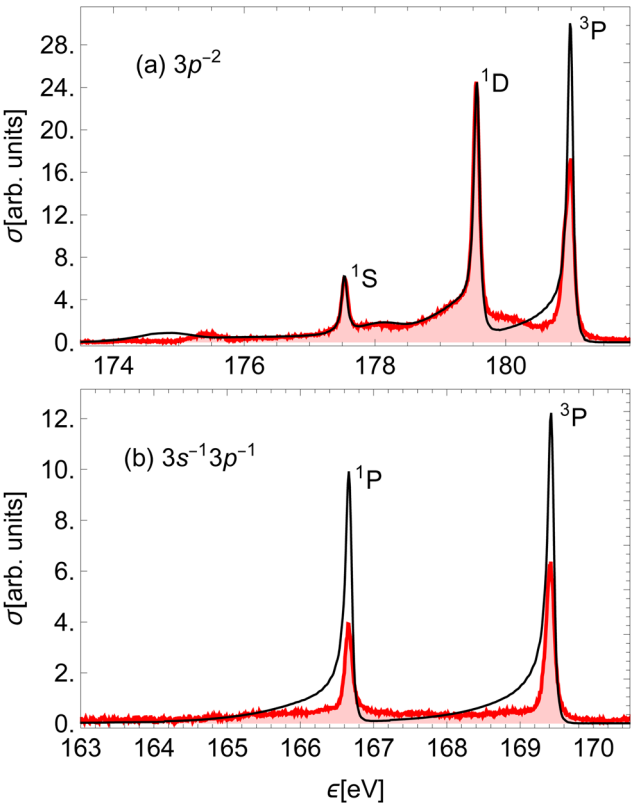

Fig. 7 Comparison of the (a) high-energy and (b) low-energy part of the calculated Auger electron spectrum (black) to the experimental result on HCl[51] (red). The calculated peaks were moved horizontally to match the corresponding experimental peaks and scaled to the (highest) ^{1}D experimental peak. Each peak is denoted by the Cl^+ final state in the dissociation limit.

achieved in the low- and high-energy parts of the spectrum. In the former, the line shapes are also not reproduced well, which is probably a consequence of using less accurate PECs.

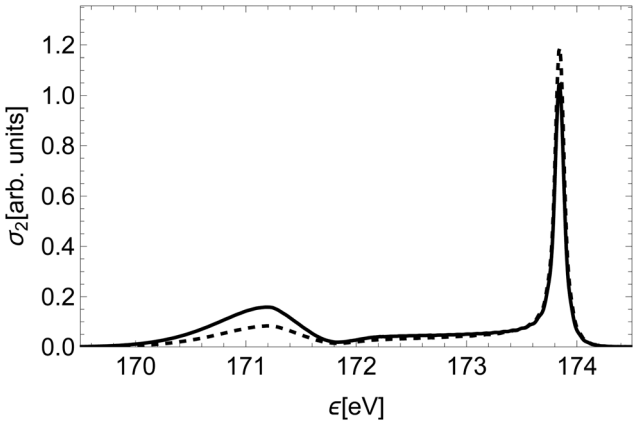

Fig. 8 Comparison of the spectral line of the state $(2)^2\Sigma^+$ (dashed) to the spectral line of the same state calculated with constant decay rates, fixed at the value of R_∞ (full).

To illustrate the significance of the varying decay rate, we compare in Fig. 8 the spectral line of the state $(2)^2\Sigma^+$ to the spectral line of the same state calculated with constant partial decay rates, fixed at the value in the atomic limit. At small inter-nuclear distances the total rate Γ_i, as well as the partial decay rates $\tilde{A}_f$, are larger in this case than in reality. This affects the relative intensity of the molecular tail compared to the high-energy atomic peak, in particular overestimating the intensity of the molecular tail.

Furthermore, we compare our quantum-mechanical treatment of nuclear dynamics to a classical approach. The latter assumes a classical dissociation dynamics based on the slope of the initial state's PEC, a smearing of the initial position based on the ground vibration state of a harmonic oscillator and a Loretzian broadening by $\Gamma_i(R)$ (similar to that of Kukk *et al.*[28]). Fig. 9 shows a striking difference between the spectral line for the state (14) obtained with the classical and quantum models. The high-energy peaks have a similar shape and width, while the low-energy part is highly over-estimated by the classical model.

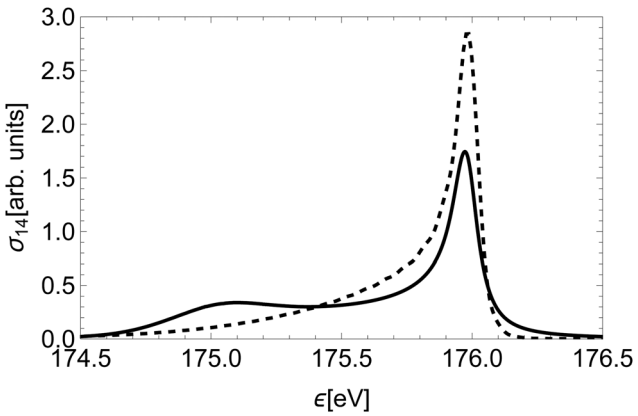

Fig. 9 The Auger spectral line of state $(14)^2\Delta$ calculated in a classical approximation (full) and the quantum-mechanical treatment of Section 2.3 (dashed).

This discrepancy stems from the fact that in the region of the low kinetic energies the nuclear part of the amplitude is significantly suppressed, while in the classical model of decay dynamics the system spends a significant amount of time in this region.

4 Conclusions

We have calculated the resonant Auger electron spectrum of the $2p_{3/2}{}^{-1}\sigma^*$ state of HCl, which undergoes ultra-fast dissociation on the same time-scale. Comparison to available experimental results shows very good agreement in the shape of spectral lines, which validates the proposed approximations for calculating such spectra. This is, to our knowledge, the first *ab initio* method that considers the variation of Auger rates during all stages of molecular dissociation, and proves the importance of this effect in describing the RA spectrum.

The quantum-mechanical description of nuclear dynamics was shown to significantly affect the shapes of the spectral lines. Considering the dependence of transition rates on the nuclear distance has further improved the shape of the low-energy tails. The total Auger rate was seen to sensitively depend on the exact values of the radial integrals R^k. On the other hand, the shape of the total spectrum is not that sensitive to these parameters. The shape of the final states' PECs in the molecular region strongly affects the shapes of the molecular tails, while the position of the atomic peak crucially depends on the corresponding dissociation limit.

Our approach works for the $2p^{-1}\sigma^*$ resonance of the HCl molecule but can also be directly applied to other molecular systems with a localized core–hole, even when the usual approximations, presented in ref. 38, are not applicable. For the results of Section 2.2 to be valid, the shapes of the spectator orbitals should not change significantly during the decay. On the other hand, the change of the participating valence orbitals in the vicinity of the core–hole is reflected in the variation of decay rates with the inter-nuclear distance. In larger molecules the orbital of a weakly bound inner-valence hole may receive more significant contributions from the neighbouring atoms than in HCl, which challenges the validity of the one-center approximation. For very large molecules the approximation of the continuum state by partial waves (see eqn (2)) is no longer valid, since the potential in which the Auger electron moves is largely distorted by other atoms and the core–hole state becomes delocalized.

The main features of the developed theory could also be applied to a participator decay, if final states populated by such decay were dissociative. However, in the presented case of the $2p^{-1}\sigma^*$ resonance in the HCl molecule the probability for participator decay to both accessible states ($X^2\Pi$ and $A^2\Sigma^+$ from ref. 29) is suppressed, and our calculation of spectator rates quite accurately reproduces the measured spectrum.

To improve the description of the final states, one could consider their L–S coupling, which should particularly improve the shape of the ^3P atomic peak, as the dissociation limit in fact

splits into three different channels by their total angular momenta J = 0, 1, and 2. Previous studies show that the distribution of intensities among these three peaks doesn't obey the statistical ratio known from atomic physics. To model this theoretically one should therefore consider the dissociation of molecular states as an interference between three possible channels. A method for this had been proposed by Lee, Williams and Freed,[52] who applied it to the OH molecule.

To improve the Auger decay rates within the one-center approximation, a more refined calculation could avoid averaging over the 2p orbitals of the initial state and explicitly consider the transition from either the $2p_{3/2}{}^{-1}\sigma^*$ state or one of the higher LS-split states. Ultimately, one would like to abandon the one-center approximation and consider a truly molecular Auger electron continuum.

Data availability

Data for this article, including potential energy curves, Auger decay rates and spectral lines, are available at ZENODO at **https://doi.org/10.5281/zenodo.13833475**.

Conflicts of interest

There are no conflicts to declare.

Acknowledgements

This publication is based upon work from COST Action CA18212 – Molecular Dynamics in the GAS phase (MD-GAS), supported by COST (European Cooperation in Science and Technology). This work was financially supported by the Slovenian Research Agency in the framework of research program P1-0112 Studies of Atoms, Molecules and Structures by Photons and Particles. Part of this work was financed by the European Research Council (ERC) through the Starting Grant No. 801770 (ANGULON). The authors acknowledge P. Lablanquie, H. Iwayama, F. Penent, K. Soejima and E. Shigemasa for sharing their unpublished experimental spectra on HCl.

References

1 P. Morin and I. Nenner, *Phys. Rev. Lett.*, 1986, **56**, 1913–1916.
2 H. Aksela, S. Aksela, M. Ala-Korpela, O.-P. Sairanen, M. Hotokka, G. Bancroft, K. Tan and J. Tulkki, *Phys. Rev. A: At., Mol., Opt. Phys.*, 1990, **41**, 6000–6005.
3 A. Menzel, B. Langer, J. Viefhaus, S. Whitfield and U. Becker, *Chem. Phys. Lett.*, 1996, **258**, 265–270.
4 E. Kokkonen, K. Jänkälä, M. Patanen, W. Cao, M. Hrast, K. Bučar, M. Žitnik and M. Huttula, *J. Chem. Phys.*, 2018, **148**, 174301.
5 D. L. Hansen, J. Cotter, G. R. Fisher, K. T. Leung, R. Martin, P. Neill, R. C. C. Perera, M. Simon, Y. Uehara, B. Vanderford, S. B. Whitfield and D. W. Lindle, *J. Phys. B: At., Mol. Opt. Phys.*, 1999, **32**, 2629–2647.
6 H. Aksela, S. Aksela, O.-P. Sairanen, A. Kivimäki, G. M. Bancroft and K. H. Tan, *Phys. Scr.*, 1992, **1992**, 122.
7 E. Pahl, L. Cederbaum, H.-D. Meyer and F. Tarantelli, *Phys. Rev. Lett.*, 1998, **80**, 1865–1868.
8 A. F. Lago, J. Z. Dávalos, U. Kerdpin and A. S. Schlachter, *J. Chem. Phys.*, 2006, **110**, 13717–13723.
9 M. Kivilompolo, A. Kivimäki, H. Aksela, M. Huttula, S. Aksela and R. F. Fink, *J. Chem. Phys.*, 2000, **113**, 662–675.
10 H. Sann, T. Havermeier, C. Müller, H.-K. Kim, F. Trinter, M. Waitz, J. Voigtsberger, F. Sturm, T. Bauer, R. Wallauer, D. Schneider, M. Weller, C. Goihl, J. Tross, K. Cole, J. Wu, M. S. Schöffler, H. Schmidt-Böcking, T. Jahnke, M. Simon and R. Dörner, *Phys. Rev. Lett.*, 2016, **117**, 243002.
11 N. Boudjemia, K. Jänkälä, R. Püttner, T. Marchenko, O. Travnikova, R. Guillemin, L. Journel, I. Ismail, D. Koulentianos, S. Kosugi, Y. Azuma, M. Patanen, M. Huttula, D. Céolin, M. N. Piancastelli and M. Simon, *Phys. Chem. Chem. Phys.*, 2020, **22**, 26806–26818.
12 O. Travnikova, T. Marchenko, G. Goldsztejn, K. Jänkälä, N. Sisourat, S. Carniato, R. Guillemin, L. Journel, D. Céolin, R. Püttner, H. Iwayama, E. Shigemasa, M. N. Piancastelli and M. Simon, *Phys. Rev. Lett.*, 2016, **116**, 213001.
13 O. Travnikova, E. Kukk, F. Hosseini, S. Granroth, E. Itälä, T. Marchenko, R. Guillemin, I. Ismail, R. Moussaoui, L. Journel, J. Bozek, R. Püttner, P. Krasnov, V. Kimberg, F. Gel'mukhanov, M. N. Piancastelli and M. Simon, *Phys. Chem. Chem. Phys.*, 2022, **24**, 5842–5854.
14 T. Marchenko, L. Inhester, G. Goldsztejn, O. Travnikova, L. Journel, R. Guillemin, I. Ismail, D. Koulentianos, D. Céolin, R. Püttner, M. N. Piancastelli and M. Simon, *Phys. Rev. A*, 2018, **98**, 063403.
15 T. Jahnke, R. Guillemin, L. Inhester, S.-K. Son, G. Kastirke, M. Ilchen, J. Rist, D. Trabert, N. Melzer, N. Anders, T. Mazza, R. Boll, A. De Fanis, V. Music, T. Weber, M. Weller, S. Eckart, K. Fehre, S. Grundmann, A. Hartung, M. Hofmann, C. Janke, M. Kircher, G. Nalin, A. Pier, J. Siebert, N. Strenger, I. Vela-Perez, T. M. Baumann, P. Grychtol, J. Montano, Y. Ovcharenko, N. Rennhack, D. E. Rivas, R. Wagner, P. Ziolkowski, P. Schmidt, T. Marchenko, O. Travnikova, L. Journel, I. Ismail, E. Kukk, J. Niskanen, F. Trinter, C. Vozzi, M. Devetta, S. Stagira, M. Gisselbrecht, A. L. Jäger, X. Li, Y. Malakar, M. Martins, R. Feifel, L. P. H. Schmidt, A. Czasch, G. Sansone, D. Rolles, A. Rudenko, R. Moshammer, R. Dörner, M. Meyer, T. Pfeifer, M. S. Schöffler, R. Santra, M. Simon and M. N. Piancastelli, *Phys. Rev. X*, 2021, **11**, 041044.
16 H. J. Thompson, O. Plekan, M. Bonanomi, N. Pal, F. Allum, A. D. Brynes, M. Coreno, S. Coriani, M. B. Danailov, P. Decleva, A. Demidovich, M. Devetta, D. Faccialà, R. Feifel, R. Forbes, C. Grazioli, D. M. P. Holland, P. Piseri, K. C. Prince, D. Rolles, M. S. Schuurman, A. Simoncig, R. J. Squibb, B. N. C. Tenorio, C. Vozzi, M. Zangrando, C. Callegari, R. S. Minns and M. D. Fraia, *J. Phys. B: At., Mol. Opt. Phys.*, 2024, **57**, 215602.
17 I. Ismail, L. Inhester, T. Marchenko, F. Trinter, A. Verma, A. De Fanis, A. Ferté, D. E. Rivas, D. Peng, D. Koulentianos,

E. Kukk, F. Penent, G. Doumy, G. Sansone, J. D. Bozek, K. Li, L. Young, M. Ilchen, M. N. Piancastelli, M. Meyer, N. Velasquez, O. Travnikova, R. Boll, R. Guillemin, R. Dörner, R. Taeb, S. Dold, S. Carniato, T. M. Baumann, T. Mazza, Y. Ovcharenko, R. Püttner and M. Simon, *Phys. Rev. A*, 2024, **110**, 013108.
18 G. Grell and S. I. Bokarev, *J. Chem. Phys.*, 2020, **152**, 074108.
19 W. Skomorowski and A. I. Krylov, *J. Chem. Phys.*, 2021, **154**, 084124.
20 B. N. C. Tenorio, T. A. VoÃŸ, S. I. Bokarev, P. Decleva and S. Coriani, *J. Chem. Theory Comput.*, 2022, **18**, 4387–4407.
21 N. K. Jayadev, W. Skomorowski and A. I. Krylov, *J. Phys. Chem. Lett.*, 2023, **14**, 8612–8619.
22 R. Bohinc, M. Žitnik, K. Bučar, M. Kavčič, L. Journel, R. Guillemin, T. Marchenko, M. Simon and W. Cao, *J. Chem. Phys.*, 2013, **139**, 134302.
23 H. Aksela, E. Kukk, S. Aksela, O. P. Sairanen, A. Kivimaki, E. Nommiste, A. Ausmees, S. J. Osborne and S. Svensson, *J. Phys. B: At., Mol. Opt. Phys.*, 1995, **28**, 4259.
24 A. Kivimäki, E. Kukk, J. Karvonen, J. Mursu, E. Nõmmiste, H. Aksela and S. Aksela, *Phys. Rev. A: At., Mol., Opt. Phys.*, 1998, **57**, 2724–2730.
25 E. Kukk, *J. Electron Spectrosc. Relat. Phenom.*, 2002, **127**, 43–51.
26 E. Sokell, A. Wills, M. Wiedenhoeft, X. Feng, D. Rolles and N. Berrah, *J. Phys. B: At., Mol. Opt. Phys.*, 2005, **38**, 1535.
27 P. Lablanquie, H. Iwayama, F. Penent, K. Soejima and E. Shigemasa, *J. Electron Spectrosc. Relat. Phenom.*, 2014, **195**, 96–100.
28 E. Kukk, H. Aksela, O. Sairanen, S. Aksela, A. Kivimäki, E. Nõmmiste, A. Ausmees, A. Kikas, S. J. Osborne and S. Svensson, *J. Chem. Phys.*, 1996, **104**, 4475–4480.
29 A. D. Pradhan, K. P. Kirby and A. Dalgarno, *J. Chem. Phys.*, 1991, **95**, 9009–9023.
30 G. Goldsztejn, R. Guillemin, T. Marchenko, O. Travnikova, D. Céolin, L. Journel, M. Simon, M. N. Piancastelli and R. Püttner, *Phys. Chem. Chem. Phys.*, 2022, **24**, 6590–6604.
31 M. O. Krause, *J. Phys. Chem. Ref. Data*, 1979, **8**, 307.
32 E. Pahl, L. S. Cederbaum, H.-D. Meyer and F. Tarantelli, *Phys. Rev. Lett.*, 1998, **80**, 1865–1868.
33 L. Inhester, C. F. Burmeister, G. Groenhof and H. Grubmüller, *J. Chem. Phys.*, 2012, **136**, 144304.
34 B. N. C. Tenorio, K. B. Møller, P. Decleva and S. Coriani, *Phys. Chem. Chem. Phys.*, 2022, **24**, 28150–28163.
35 E. Z. Chelkowska and F. P. Larkins, *At. Data Nucl. Data Tables*, 1991, **49**, 121–206.
36 R. F. Fink, M. Kivilompolo, H. Aksela and S. Aksela, *Phys. Rev. A: At., Mol., Opt. Phys.*, 1998, **58**, 1988–2000.
37 H. Siegbahn, L. Asplund and P. Kelfve, *Chem. Phys. Lett.*, 1975, **35**, 330–335.
38 F. Gelmukhanov and H. Ågren, *Phys. Rev. A: At., Mol., Opt. Phys.*, 1996, **54**, 379–393.
39 K. Hermann, L. G. M. Pettersson, M. E. Casida, C. Daul, A. Goursot, A. Koester, E. Proynov, A. St-Amant, D. R. Salahub, V. Carravetta, H. Duarte, C. Friedrich, N. Godbout, M. Gruber, J. Guan, C. Jamorski, M. Leboeuf, M. Leetmaa, M. Nyberg, S. Patchkovskii, L. Pedocchi, F. Sim, L. Triguero and A. Vela, *StoBe-deMon version 3.3*, 2014.
40 J. P. Perdew and W. Yue, *Phys. Rev. B: Condens. Matter Mater. Phys.*, 1986, **33**, 8800–8802.
41 J. P. Perdew, K. Burke and M. Ernzerhof, *Phys. Rev. Lett.*, 1996, **77**, 3865.
42 D. E. Woon, J. Dunning and H. Thom, *J. Chem. Phys.*, 1993, **98**, 1358–1371.
43 S. Huzinaga, *J. Chem. Phys.*, 1965, **42**, 1293–1302.
44 F. Gel'mukhanov, H. Ågren, S. Svensson, H. Aksela and S. Aksela, *Phys. Rev. A: At., Mol., Opt. Phys.*, 1996, **53**, 1379–1387.
45 L. D. Landau and L. M. Lifshitz, *Quantum Mechanics Non-Relativistic Theory*, Butterworth-Heinemann, 3rd edn, 1981, vol. 3.
46 *NIST Computational Chemistry Comparison and Benchmark Database*, 2022, **https://cccbdb.nist.gov/**, [Online; accessed 27. 4. 2023].
47 C. Froese-Fischer, *Computational Atomic Structure: An MCHF Approach*, 1st edn, 1997.
48 P. Jönsson, X. He, C. F. Fischer and I. P. Grant, *Comput. Phys. Commun.*, 2007, **177**, 597–622.
49 P. W. Atkins and R. S. Friedman, *Molecular Quantum Mechanics*, Oxford University Press, 3rd edn, 1996.
50 F. Gel'mukhanov and H. Ågren, *Phys. Rep.*, 1999, **312**, 87–330.
51 P. Lablanquie, *private communication*, 2023.
52 S. Lee, C. J. Williams and K. F. Freed, *Chem. Phys. Lett.*, 1986, **130**, 271–277.